Materials Advances

ROYAL SOCIETY OF CHEMISTRY

PAPER

View Article Online
View Journal | View Issue

Cite this: *Mater. Adv.*, 2022, 3, 8977

Unexpected behavior during methylene blue adsorption over H-titanate nanotubes and nanosheets

A. H. Zaki, *[ab] Shimaa Rashad,[b] Ming-Jer Lee [a] and Nabila Shehata[c]

Received 7th March 2022,
Accepted 30th September 2022

DOI: 10.1039/d2ma00267a

rsc.li/materials-advances

2D titanate nanosheets (H-TNS) and 1D titanate nanotubes (H-TNT) were synthesized by using a simple hydrothermal technique to effectively adsorb cationic methyl blue (MB) dye from aqueous solutions. These nanomaterials were characterized by X-ray diffraction (XRD) and transmission electron microscopy (TEM). The effects of pH values, contact time, and the initial concentration of the dye on the adsorption behavior were investigated. The studies on the equilibrium and the kinetic behavior of adsorption are also included in this work. Various equilibrium adsorption models (including the Langmuir and the Freundlich models) and kinetic models were adopted to correlate the experimental data taken in the present study. The results showed that the adsorption capacity of methylene blue was 7.25 mg g^{-1} and 6.67 mg g^{-1} for H-TNT and H-TNS, respectively. Moreover, the effects of the morphology of titanate, the initial concentration of the dye, and the temperature of the solution on the chromatic behavior of cationic methylene blue dye were investigated. Finally the reusability of the nanomaterials was also tested.

1. Introduction

Due to the increasing growth of urbanization and industrialization, large amounts of industrial dyes are discharged from numerous industries, such as cosmetic, pharmaceutical, textile, leather, food, and paint industries. These dyes, which include more than 10 000 types, are harmful to the environment and human beings.[1,2] Moreover, dyes can be teratogenic, mutagenic or carcinogenic which can cause severe damage to humans. In particular, the organs most sensitive to dye contamination are the kidneys, brain, liver and the central nervous and reproductive systems. The major challenge is the resistance to degradation of these dyes as well as their toxicity due to the existence of toxic constituents such as amines. Due to their negative impacts on humans and ecosystems, removing or lowering the concentration of these dyes is gaining much interest. Therefore, focus on innovative techniques and materials to scavenge dyes from wastewater streams is preferable.[3]

Methylene blue (MB) is an azo dye with a heterocyclic aromatic cation structure that is commonly used in the textile industry. Because of its complex aromatic structure, it is difficult to break down using traditional biological treatment methods.[4,5] To solve these problems, many research groups have developed various methods including coagulation, ozone oxidation, photocatalytic oxidation, Fenton oxidation, magnetic separation, and adsorption.[6] One of the most efficient and cost-effective methods is adsorption. The dye molecules in the solution phase transfer to the surface of the adsorbent *via* the adsorption process. With the rapid advancement of nanotechnology in recent years, it is a common practice to use nanomaterials in environmental applications.[7–9]

Incorporation of nanotechnology to the traditional adsorption method forms an effective route to economically treat large volumes of wastewater.[3] This is attributed to the promising properties of nanoparticles used in water treatment. Due to their promising characteristics, such as high surface area, nanosize, high reactivity, mobility solution, good mechanical properties, high porosity, and dispersibility, nanomaterials have proven their efficiency in treating wastewater from numerous pollutants.[7–9] These nanoparticles can be engineered to be in the form of different morphologies including nanospheres, nanosheets, nanotubes, *etc.*[6–8] The adsorption of dyes by nanomaterials has also attracted the attention of researchers. The use of nanoparticles as adsorbents has increased during the last decade, due to their high surface area and morphology control compared to bulk materials.[10–14] Among these nanomaterials, titania and titanate nanostructures still attract attention from all researchers, because they are non-toxic, commercially available, and also their size and shape can be

[a] *Department of Chemical Engineering, National Taiwan University of Science and Technology, 43 Keelung Road, Section 4, Taipei 106-07, Taiwan. E-mail: ayman.zaki@psas.bsu.edu.eg*
[b] *Materials Science and Nanotechnology Department, Faculty of Postgraduate Studies for Advanced Sciences, Beni-Suef University, Beni-Suef, Egypt*
[c] *Environmental Science and industrial development Department, Faculty of Postgraduate Studies for Advanced Sciences, Beni-Suef University, Beni-Suef, Egypt*

Table 1 Maximum adsorption capacities of titanate materials for MB at different process parameters where the adsorption capacity is in mg g^{-1}, temperature is in °C, time is in min and concentration is in mg L^{-1} unless another unit is mentioned

Adsorbent	Temp.	Initial concn	Equilibrium time	pH	Adsorption capacity	Ref.
Sodium titanates	25	50–300	120	7	52.8–51.8	22
Titanate nanotubes sensitized with zinc tetra(4-carboxyphenyl) porphyrin	300	20	15	6	96.5	23
Graphene-titanate nanocomposite	25	10–100	1440	7	270.27	24
Titanate nanotubes	—	5–50	—	—	5.6–8.2	25
H-TNT	Room temp.	100	90	7	7.25	This study
H-TNS					6.67	

easily manipulated. These nanomaterials have unique physico-mechanicals properties, such as large surface area and porosity, which yields much more –OH sites, high stability, and ion-exchange characteristics as well as low-cost of production.[3,6,7] Recently layered titanate nanostructures have attracted more attention because of their ability to exchange cations with dyes and heavy metals.[15–17] 1D and 2D titanate nanostructures are ideal candidates for dye removal because of the high surface area and exchange ability compared to bulk titania and titanate.[18–20] Recently, titante showed promising results for the removal of different dyes.

However, previous investigations related to titanate nanotubes focused on the synthesis, structure characteristics and evaluation of the developed catalysts in photocatalysis, but little attention was given to studying the characteristic adsorption of organic materials onto titanate. Yuan *et al.*[21] prepared and applied titanate nanosheets for MB adsorption. They noticed for the first time that at certain concentrations, MB molecules desorb to form dimers and trimers. In our work, as a representative of organic azo pollutants, MB, which is widespread in industrial wastewater, was used. The adsorption capacity of H-TNT and H-TNS toward MB was evaluated. The adsorption kinetics data were correlated with the Langmuir and the Freundlich models. Several studies reported on the synthesis of titante nanosheets as well as their adsorption activity, but no study was made on investigating the correlations for the adsorption behavior of MB onto 1D and 2D titanate nanostructures at different initial concentrations of MB and temperature. A comparison of the MB adsorptive characteristics onto different titante materials is shown in Table 1.

2. Materials and methods

2.1 1D and 2D titanate preparation and characterization

The reagents used in this study were bought from Sigma-Aldrich and used directly. Methylene blue ($C16H18ClN3S{\cdot}XH2O$ [X = 2, 3]) was supplied from General Drug House (P) Ltd, (India), and the chemical structure of MB is illustrated in Scheme 1. H-titanate nanosheets (2D) and nanotubes (1D) were prepared using a simple hydrothermal method, as in our recently published work.[6] In a typical synthesis, 10 g of powder titania nanoparticles were mixed with 10 N NaOH for 30 min until a milky-white suspension was obtained, and the suspension was then transferred into a Teflon-lined autoclave with a vessel capacity of about 1000 mL. The autoclave was subject to heating in an oven at 160 °C for 6 and 20 h to obtain the nanosheets (H-TNS) and nanotubes (H-TNT), respectively. The autoclave was allowed to cool down to room temperature, and then the white powders formed were washed several times with distilled water, and then with 0.1 M HCl under sonication. At the end all samples were placed in a muffle furnace at 500 °C for 4 h. The prepared titanate was characterized using high-resolution transmission electron microscopy (HRTEM) micrographs obtained from a JEOL-JEM 2100 (Japan) with an acceleration voltage of 200 kV. X-ray diffraction (XRD) patterns were recorded on a PANalytical (Empyrean) XRD using Cu Ka radiation (wavelength 0.154 cm^{-1}) at an accelerating voltage of 40 kV, current of 35 mA, scan angle range of 5–80, and scan step of 0.02°. The zeta potential was measured using a Zetasizer Nano-ZS90 (Malvern, UK). The Brunauer–Emmett–Teller (BET) surface area was measured by N_2 adsorption using a Micromeritics TriStar II.

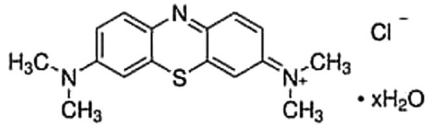

Scheme 1 Chemical structure of MB.

2.2 Adsorption study

A 200 ppm stock solution of methylene blue was prepared by dissolving the powder in distilled water, and different concentrations of methylene blue were prepared by diluting in certain volumes of the stock solution; solutions of 5, 10, 25, 30, 40, and 50 ppm were prepared. The adsorption experiments were performed in a glass batch-reactor, and the circulated water from the thermostatic bath maintained the temperature. The effect of temperature was studied at certain concentrations to evaluate their action on dimer and trimer formation. The removal efficiency was followed-up by withdrawing samples (500 μL) at certain time intervals, separating by gravitational force, and analyzing them using Jasco, V-300, UV-Vis. Spectrophotometer.

3. Results and discussion

3.1 Titanate characterization

HRTEM images as shown in Fig. 1 confirm the successful preparation of the desired titanate nanosheets and nanotubes.

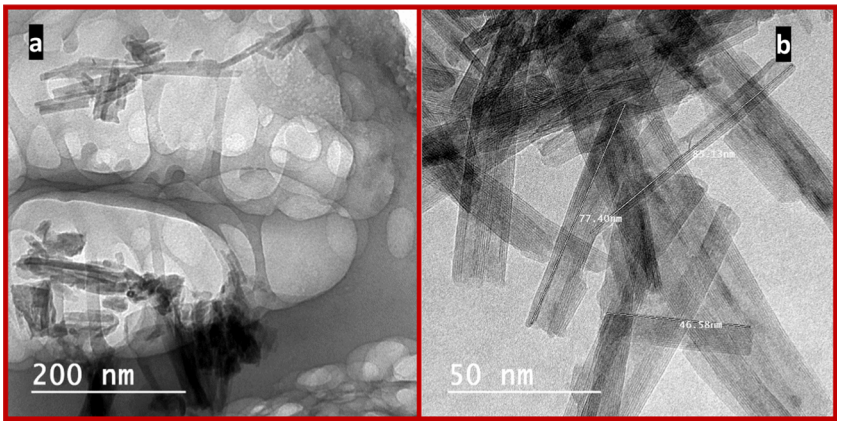

Fig. 1 HRTEM images of (a) H-TNS and (b) H-TNT.

In Fig. 2a, the multilayered nanosheets can be observed; the nanosheets are stacked with each other and are not uniform in size. While the nanotubes are shown in Fig. 2b, the tubular structure with internal cavities are clear in all tubes, and all tube diameters are less than 10 nm.

Fig. 2 shows the recorded XRD patterns of H-TNS and H-TNT, the observed reflections of nanosheets at 2θ; 5.6°, 10.6° 25.3°, 29.6°, 44.1°, and 48.3° (Fig. 2a) were compared with [ICDD card no. 01-077-4140] of the monoclinic phase of dihydrogen trititanate ($H_2Ti_3O_7$), while the reflections of H-TNT

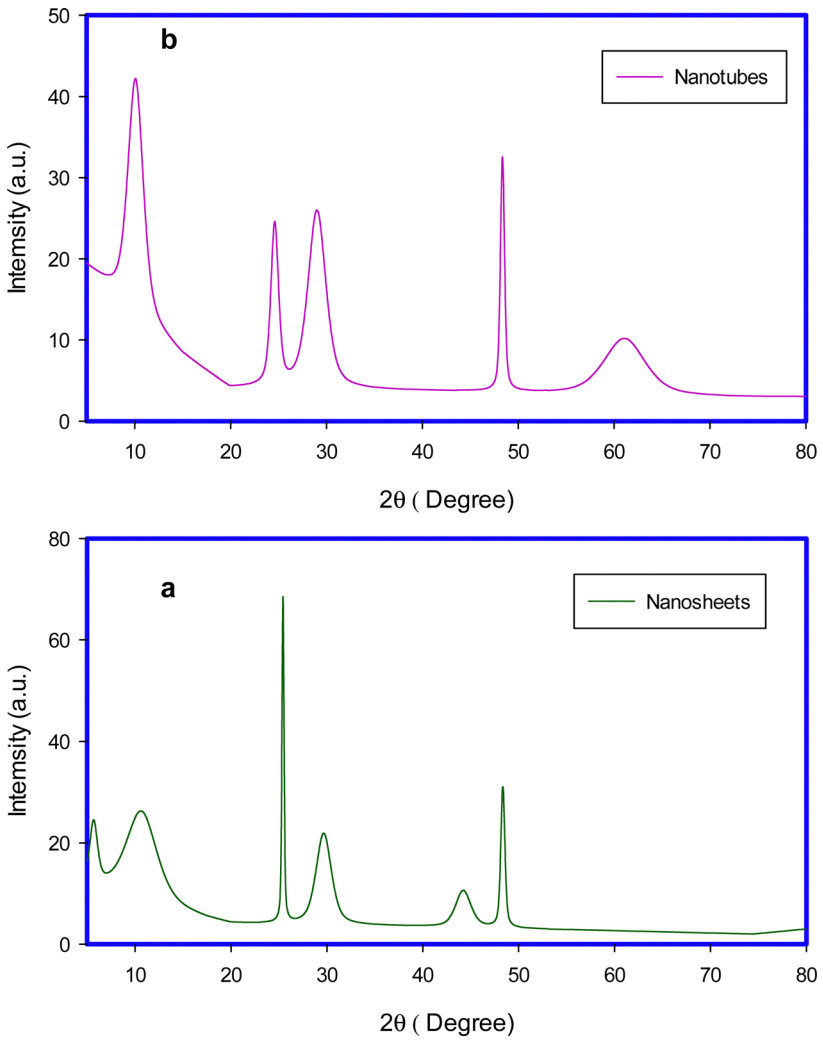

Fig. 2 XRD patterns of (a) H-TNS and (b) H-TNT.

Table 2 Summary of the obtained data for H-TNS and H-TNT; surface areas, pore volumes, and pore sizes

Morphology	BET ($m^2\ g^{-1}$)	Pore volume ($cm^3\ g^{-1}$)	Pore size (nm)
Nanosheets	72	0.085	4.8
Nanotubes	83	0.1305	5.8

were observed at 2θ; 9.8°, 24.2°, 28.2°, 48.2°, 61.7°), and were found to coincide with [ICDD card no. 00-047-0124], of hydrogen titanium oxide hydrate nanotubes.

Surface areas, pore volumes, and pore sizes were obtained and are listed in Table 2. For titanate nanotubes, the surface area is 83 $m^2\ g^{-1}$, pore volume is 0.1305 $cm^3\ g^{-1}$, and pore size is 5.8 nm. On the other hand, for the nanosheets these values are 72 $m^2\ g^{-1}$, 0.085 $cm^3\ g^{-1}$, and 4.8 nm, respectively. It is clear from the results that the nanotubes are higher in their specific surface area and pore width and volume by 13.25, 34.9 and 17.2%, respectively, compared to the nanosheets. This is due to the fact that the development of the nanomaterial in tube geometry increased their internal surface area rather than the sheet configuration.[6]

3.2 Adsorption study

3.2.1 Effect of pH. Dye adsorption processes are greatly affected by the pH of solutions, since the surface charge of the adsorbent is changed with pH, and affects the ionization of the adsorbate. As shown in Fig. 3, the zeta potential values at different pH values suggest that the obtained values for H-titanate nanotubes and nanosheets were found to be close to each other at different pH values, except for at pH 5, where the charge of the nanosheets was −24 and −11 for nanotubes. The removal % of methylene blue over H-TNS and H-TNT

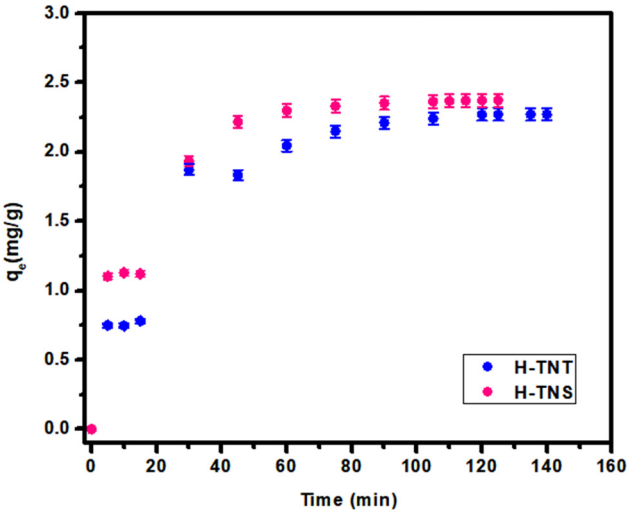

Fig. 4 Effect of time on the adsorptivity of MB (10 ppm) onto H-TNS and H-TNT.

significantly increased by increasing the pH values, which is attributed to the change in zeta potential values with increasing pH where at higher pH values, the density of the negative charges on the adsorbent surface increased which increased the tendency of the adsorbent for the attraction of the cationic methylene blue.

Hence, the adsorption mechanism might be attributed mainly to the electrostatic attraction between the MB and sorbents under investigation. This is in agreement with ref. 26, in which it was also reported that the adsorption was basically controlled by electrostatic forces.

However, titanate developed using a hydrothermal synthesis route is characteristic with an ion-exchange property which

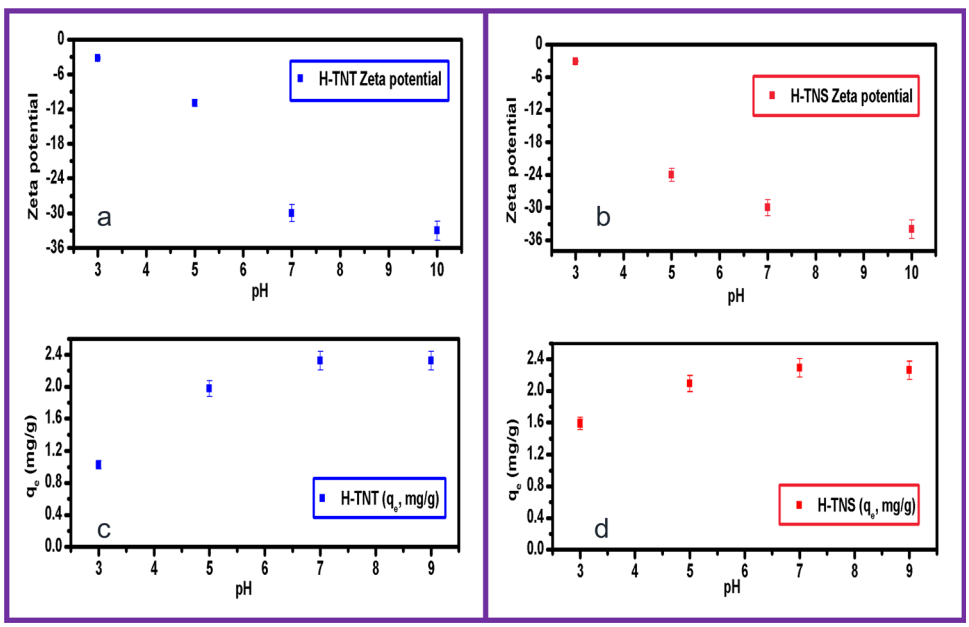

Fig. 3 Zeta potential at various pH values for H-TNT (a) and H-TNS (b) and the effect of pH on the adsorption of MB onto H-TNT (c) and H-TNS (d) at V 25 ml, adsorbent mass 0.1 g and Co = 10 mg L^{-1} (b).

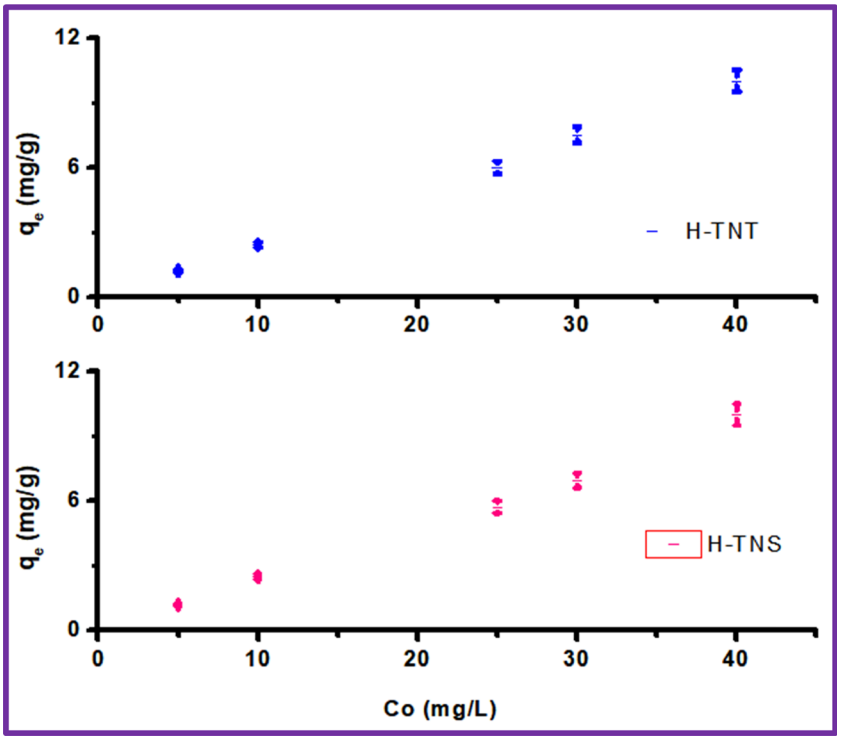

Fig. 5 Effect of the dye initial concentration on the MB adsorption onto H-TNT and H-TNS.

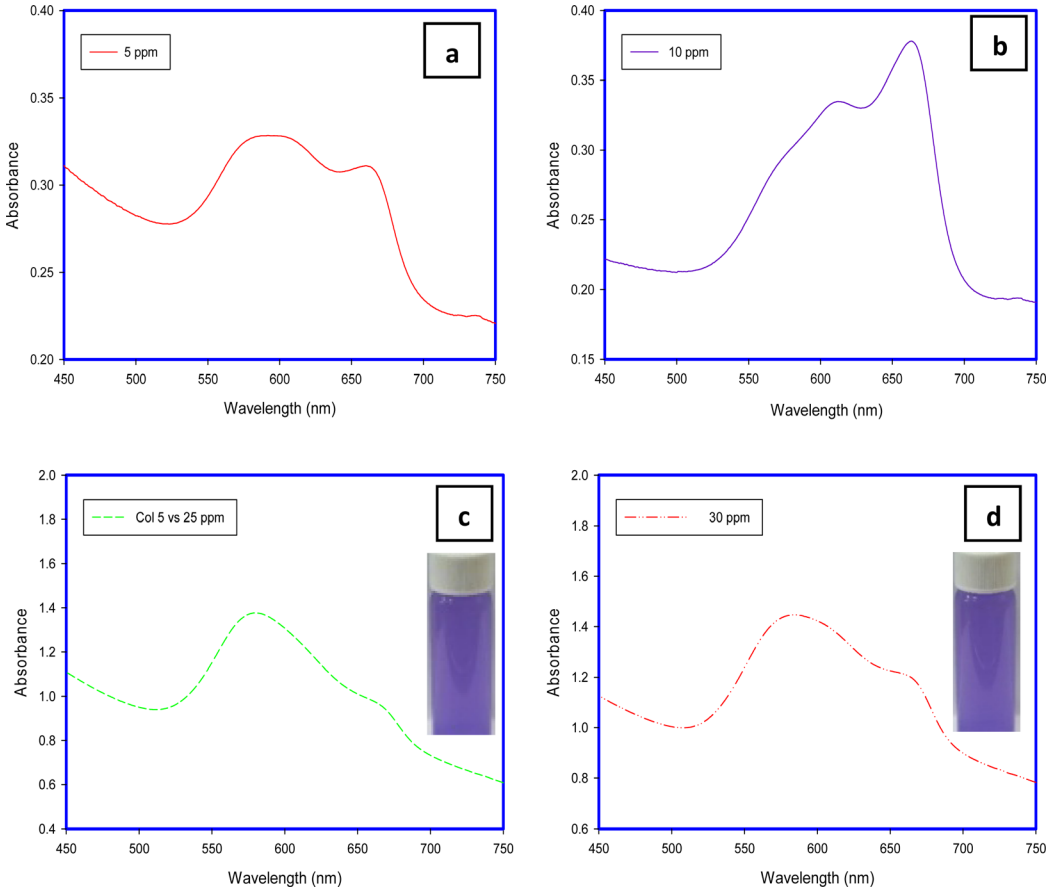

Fig. 6 UV-Visible spectra of different concentrations of MB after removal using H-TNT.

encourages the sorption of basic dyes such as MB *via* a cation exchange mechanism.[27]

Although there is a difference in the surface area between the two adsorbents, the efficiency is too close, which is may be attributed to the preferred orientations in the crystal structure of H-TNS and H-TNT, as found in our recent study.[6]

3.2.2 Effect of contact time in H-TNS and H-TNT. The effect of contact time on the adsorption of methylene blue over titanate nanosheets and nanotubes is illustrated in Fig. 4, and the results reveal that the adsorption capacity increased with time and it reached equilibrium in 90 min. in both cases. Increasing the time above this time doesn't significantly affect the adsorption process.

3.2.3 Effect of the initial dye concentration on the adsorption process. The MB adsorptivity onto H-TNT and H-TNS showed a considerable increase with increasing the initial concentration of the MB (Fig. 5). This is due to the fact that the surface area of the nanomaterials under study allow a greater concentration of the cationic MB to be adsorbed on their surfaces. However, the adsorptivity values for both morphologies are similar although the surface area of H-TNT is higher than that of H-TNS, which may have attributed to the fact that the repulsion forces between MB molecules that crowded or sandwiched between the tube surfaces/edges increase in the case of the tube geometry which affect their adsorptivity.

3.3 The chromatic behavior of MB

MB aggregation is most encouraged in water due to its methachromic characteristic in addition to the high dielectric constant of water which minimizes the electrostatic repulsion among dye molecules. This phenomenon depends on some factors such as temperature, dye concentration, ionic strength, and solvent dielectric.[28]

3.3.1 Effect of MB initial concentration on its chromatic behavior after adsorption onto H-TNT. The chromatic behavior of MB after adsorption onto H-TNT was studied over the range from 5 mg L^{-1} up to 30 mg L^{-1} (Fig. 6a–d). The MB is characterized with an absorbance band in the low energy region (at 668 nm) in addition to a shoulder around 600–610 nm which corresponds to the vibration transition from zero-ground state to 1-ground state. Their locations may vary due to some factors such as pH, temperature and the initial concentration of the dye. The presence of dimers depends on the initial concentration, temperature and hydrophobic interactions.

The band around 668 nm is present with low intensity at low concentrations (5 and 25 mg L^{-1}) and also at a high concentration (30 mg L^{-1}). In contrast to that at an initial concentration of 10 mg L^{-1}. This may be attributed to the tendency of the MB molecule to excise in dimer form at specific concentrations. For example, Huiyu Yuan stated that the dimers are present more than monomers at a concentration of 10^{-3} mol L^{-1} while

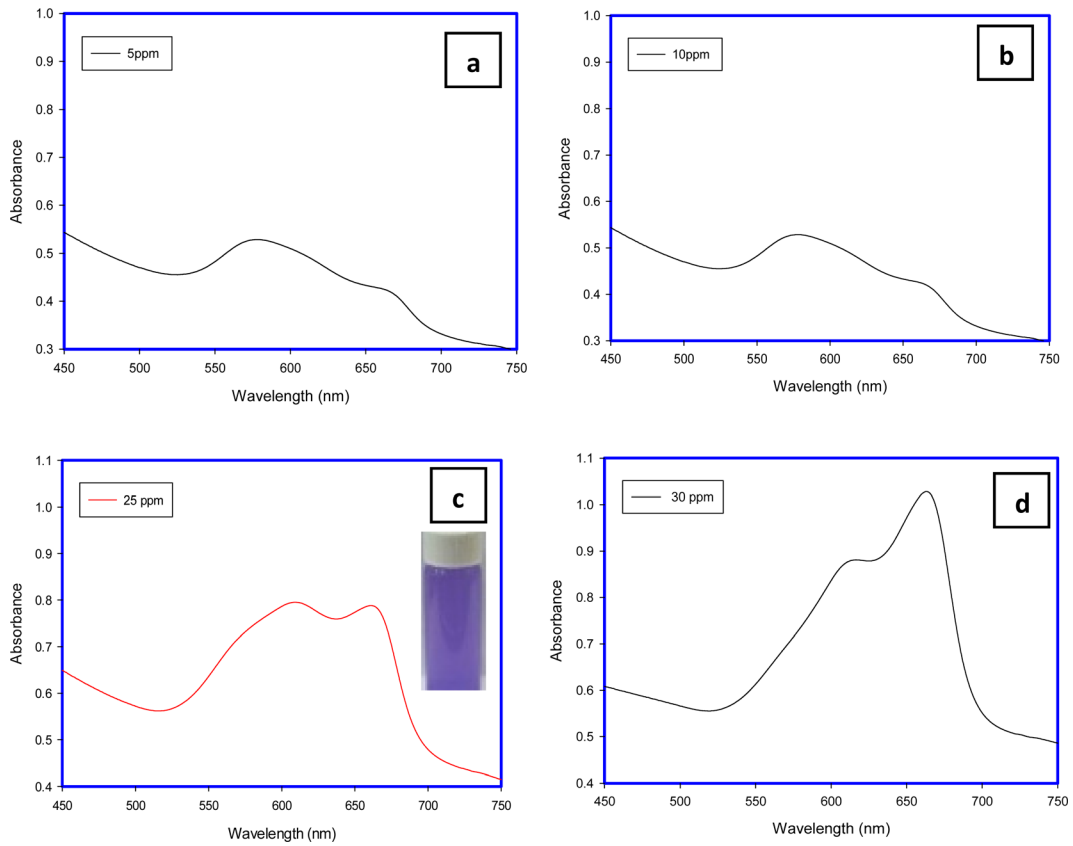

Fig. 7 UV-Visible spectra of concentrations of 5 (a), 10 (b), 25 (c) and 30 (d) mg L^{-1} of MB after removal using H-TNS.

the monomers are present more than dimers at a concentration of 10^{-7} mol L^{-1}.[21]

The shapes of the band and the shoulder refer to the fact that the monomers are the predominant species present at a concentration of 10 mg L^{-1}. At lower than this value (5 mg L^{-1}) and at higher concentrations ($\geq$25 mg L^{-1}), the dimers are dominant in the dye solution which is in line with ref. 29.

3.3.2 Effect of the initial MB concentration on its chromatic behavior after adsorption onto H-TNS. Fig. (7a–d) show the MB solution after sorption onto H-TNS, and it is clear that as the concentration increases, the spectrum of the dye changes. Increasing the initial concentration from 5 to 10 ppm doesn't affect the spectra, where the shoulder remains around 560 nm and part of the band appears at 668 nm. However, the band shape is still undefined to some extent. Fig. 7c shows that increasing the initial concentration of the dye changes the spectra where the band begins to appear clearly and finally the band at low energy becomes clear and more defined like the shoulder. Both of them appear in the same intensity. It is also observed that the intensity of the band refers to the fact that the monomers are the predominant in the case of higher concentration (30 mg L^{-1}).

The dimensions of the MB molecule are close to a rectangular shape with dimensions of 1.70 × 0.76 × 0.33 nm, compared to H-TNS, and the morphology of the H-TNS sheets facilitates the stacking of MB molecules above each other or face each other to form dimers, and subsequently the ratio monomers will increase compared to the dimer in the

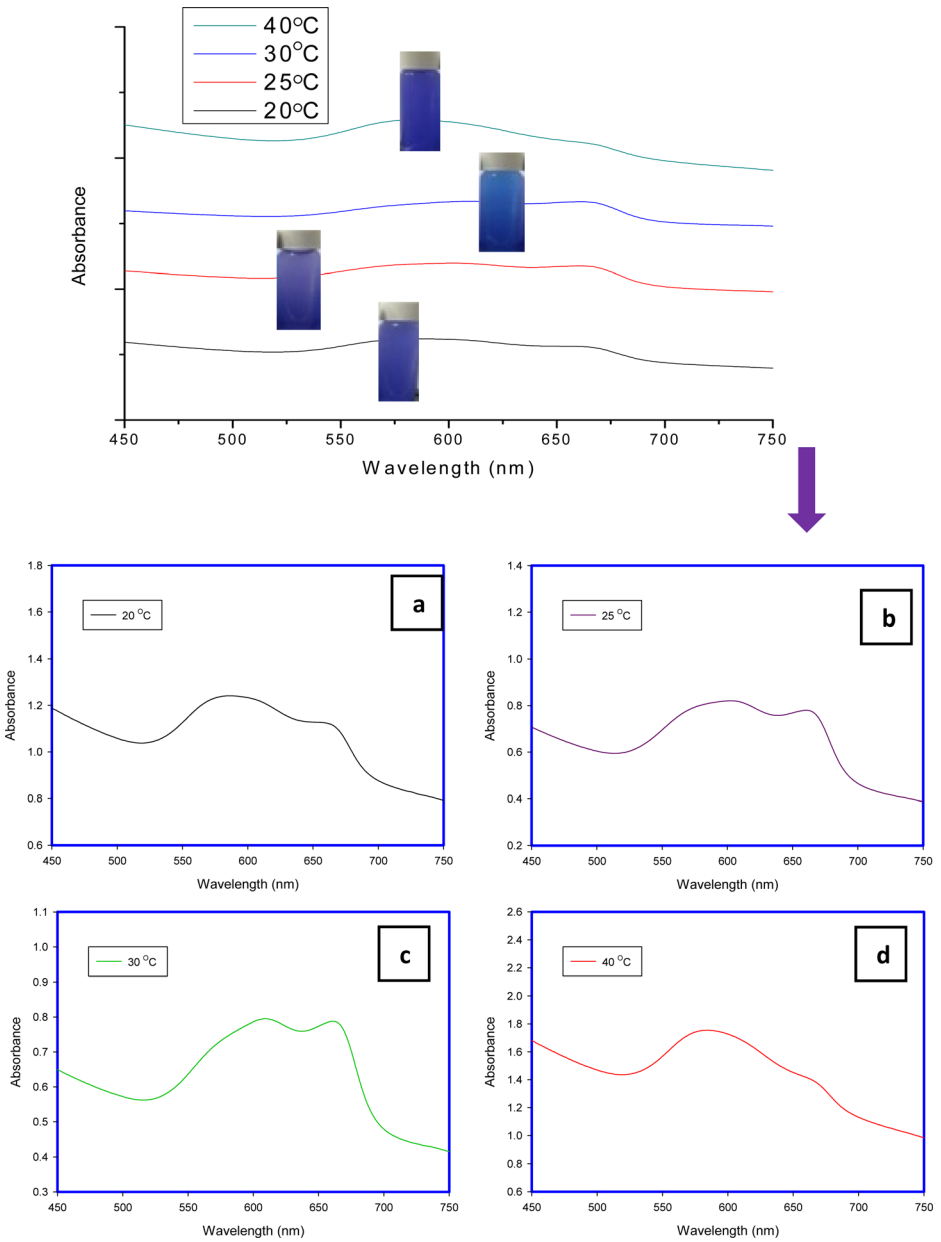

Fig. 8 UV-Visible spectra of 25 ppm solution of MB after removal using H-TNS at different temperatures: (a) 20 °C, (b) 25 °C, (c) 30 °C and (d) 40 °C.

remaining solution (MB after adsorption). And the morphology of the nanomaterials plays an important role as adsorbents.

The mechanism of MB sorption onto H-TNS and H-TNT due to ion exchange between inter-layered (H^+) and MB cations in addition to complexation due to the abundance of negative charge on the sorbent surface.

3.3.3 Effect of temperature on the MB chromatic behavior after adsorption onto H-TNS. The morphology of titanate as sheets was used to investigate the effect of temperature on the MB chromatic behavior due to its simplicity. Fig. (8a) shows that the band appears around 668 nm with low intensity and the shoulder also appears around 580 at a temperature of 20 °C, increasing the temperature of the adsorption process up to 25 °C leading to an increase in the intensity of the band and the shoulder becomes wider. The band intensity increased slightly at a temperature of 30 °C while increasing the temperature up to 40 °C decreases the band intensity significantly in the low energy region while the shoulder becomes clearer and wider. This may be due to the fact that increasing the temperature changes the solution energy and transmits the dye molecule from an energy state to a higher one. Also, the water polarity and hydrophobic interactions are the controlling parameters in the MB aggregation, so the above recorded changes in dimerization (Fig. 6 and 7) aim at aggregate equilibrium. Furthermore, it can be summarized that increasing the temperature of the MB solution >40 °C is not recommended for MB detection in water, since the dye molecules tend to stack on each other and the detected absorbance will not be accurate.

3.4 Adsorption isotherm

Langmuir and Freundlich models have been widely applied to describe the adsorption systems as the following equations:[30,31]

$$\text{Langmuir: } C_e/q_e = C_e/q_m + 1/q_e{\cdot}K_L \quad (1)$$

$$\text{Freundlich: } \log q_e = (1/n){\cdot}\log C_e + \log k_F \quad (2)$$

where C_e is the final concentration of MB in the solution after adsorption, q_m and/q_e are the maximum and at equilibrium adsorptivities, K_L and n are the Langmuir and Freundlich constants and (k_F) is the maximum adsorption capacity according to the Freundlich model.

As shown in Fig. 9 and Table 3, and based on the correlation coefficients (R^2 0.95–0.98) the Freundlich model is more suitable for MB adsorption onto H-TNT and H-TNS. The Langmuir model is not suitable for the adsorption of H-TNS (R^2 0.61) and this attributed to the fact that this model is based on the assumption that the adsorption sites of the adsorbent are energetically equivalent and there is no interaction between the adjacent adsorbed molecules and this couldn't occur since the sheets encourage MB dimerization on its surface which agreed with the above results. In contrast to H-titante nanotubes (R^2 0.82) where this phenomena is minimized.

Table 3 also shows the parameters of the non-linear modeling for the adsorption of MB onto the sorbents under study. The results show that the non-linear models can't describe the process where the correlation coefficient values are very low or negative and the calculated values of q are very high.

3.5 Kinetic studies

Five kinetic models were investigated in order to clear the MB mechanism and rate of MB adsorption onto titanate nanomaterials as follows:

Pseudo 1st order model:[32] $\text{Log}(q_e - q_t) = \log q_e - (K_1/2.303){\cdot}t$

Pseudo 2nd order model:[33] $t/q_t = [1/(k_2{\cdot}q_e^2)] + t/q_e$

Intraparticle diffusion model:[34–36] $q_t = k_i t^{0.5} + c$

Avrami model:[35,37] $q_t = q_e{\cdot}[1 - \exp[-k_{AV}{\cdot}t]^{nAV}]$

Mixed 1st and 2nd order model: $q_t/q_e = [1 - \exp(-k_1 t)]/[(1 - f_2 - \exp(-k_1 t)]$where q_e refers to the equilibrium adsorption capacity (mg g^{-1}), and q_t is due to the adsorption capacity (mg g^{-1}) at time (t), K_1 is the pseudo 1st order rate constant (min^{-1}), K_2 is the pseudo 2nd order rate constant (g mg^{-1} min^{-1}), K_i is the intraparticle diffusion rate constant (mg g^{-1} $min^{-0.5}$), c is the intercept related to the thickness of the boundary layer, k_{AV} and n_{AV} are the constants (min^{-1}) and

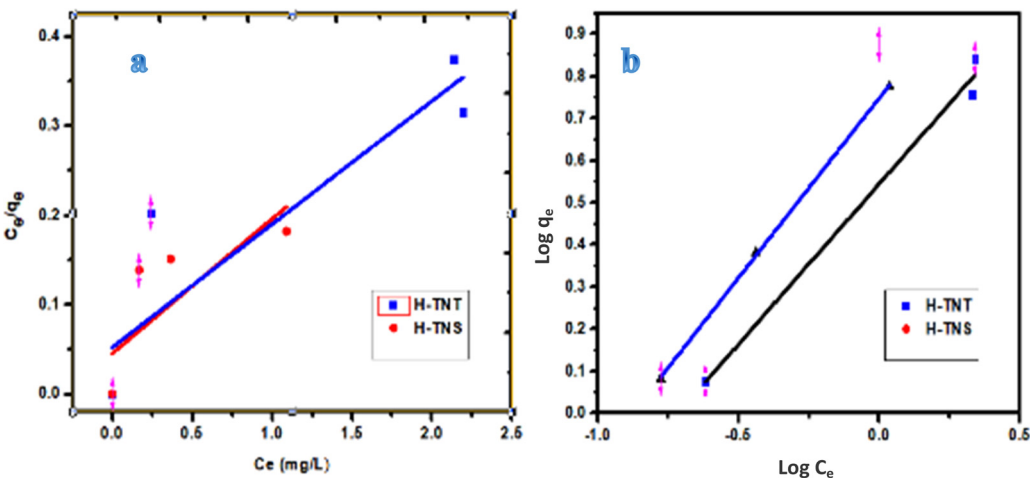

Fig. 9 Modeling of the MB adsorption process onto H-TNT and H-TNS using Langmuir (a) and Freundlich (b) models.

Table 3 The parameters of the adsorption isotherm models for the adsorption of MB onto H-TNT and H-TNS

Linear models

Model	Langmuir			Freundlich		
Parameter	K_e	q_m	R^2	K_F	n	R^2
H-TNT	2.63	7.25	0.82	3.2	1.76	0.95
H-TNS	0.007	6.67	0.61	6.4	1.068	0.98

Non-linear models

	Langmuir			Freundlich			Redlich–Peterson			
Parameter	K_e	q_m	R^2	K_F	n	R^2	K_R	a_R	b	R^2
H-TNT	0.34	14.98	0.68	3.48	1.3	0.68	54.5	14.63	0.24	0.68
H-TNS	0.004	4722	0.6	57453	0.2	0.99	0.94	0.006	1.15	−1.03

exponent (−) of the Avrami equation and f_2 refers to the constant of the mixed 1st and 2nd order model.

Based in the results illustrated in Fig. 10 and Table 4, the pseudo first order is fit to the data with high correlation coefficient (R^2) values of 0.97 and 0.95 for H-TNT and H-TNS, respectively. Additionally the calculated maximum capacity for adsorption is very close to the experimental values. Although modeling of the system using the pseudo 2nd order model yields high R^2 (0.96) the theoretical maximum adsorption values are higher than those for the experimental values. In the case of the intraparticle diffusion models, the calculated values of adsorption capacities are far away from the experimental one beside lower values of the correlation factor (R^2, 0.87–0.89).

The three parameters-models were also investigated. As shown in Fig. 11, the Avrami model could describe the adsorption process under study with high accuracy according to the values of R^2 (0.95–0.97) and matching the calculated values to that of the experimental one. The mixed 1st and 2nd order kinetic model was similar to the pseudo 2nd order, where the calculated capacities for MB adsorption into the nanosheets and tubes are higher than the experimental one while the correlation coefficient is high (0.90–0.96).

In conclusion, the adsorption process of MB onto H-TNT and H-TNS is well described using pseudo 1st order and Avrami models. Pseudo 2nd order and the mixed 1st and 2nd order

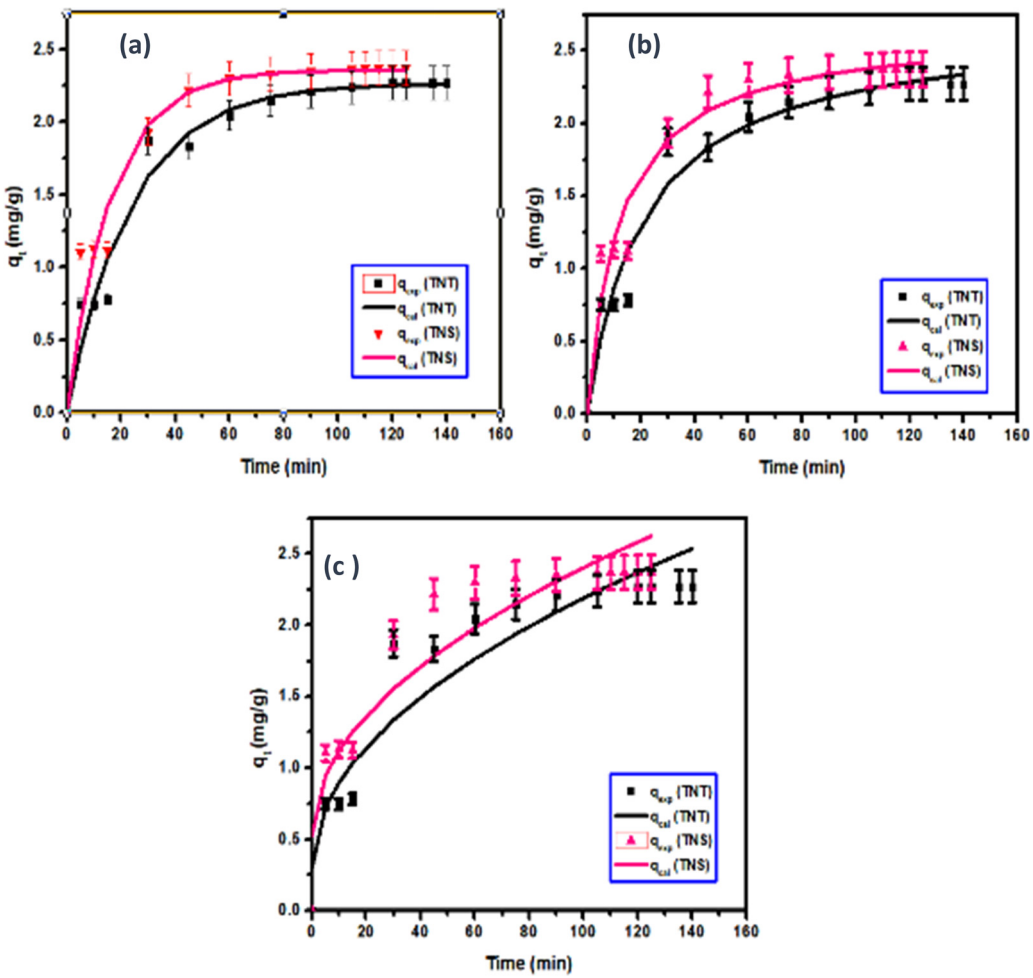

Fig. 10 Fitting of the two parameters-models: pseudo first order, pseudo second order and intraparticle diffusion models to the experimental data for the adsorption of MB onto H-TNT and H-TNS.

Table 4 The parameters of kinetic models for the MB adsorption onto H-TNT and H-TNS

Pseudo-first-order				
Material	$q_{e,exp}$ (mg g^{-1})	k_1 (min^{-1})	$q_{e,cal}$ (mg g^{-1})	R^2
H-TNT	2.27	0.042	2.27	0.97
H-TNS	2.37	0.061	2.36	0.95

Pseudo-second-order				
Material	$q_{e,exp}$	k_2 (g mg^{-1} min^{-1})	$q_{e,cal}$	R^2
H-TNT	2.27	0.018	2.68	0.96
H-TNS	2.37	0.031	2.65	0.96

Intraparticle diffusion				
Material	$q_{e,exp}$	K_{ip} (mg g^{-1} min$^{-0.5}$)	C_{ip} (mg g^{-1})	R^2
H-TNT	2.27	0.189	0.30	0.89
H-TNS	2.37	0.188	0.53	0.87

Mixed 1st and 2nd order					
Material	$q_{e,exp}$	K	q_e (mg g^{-1})	f_2	R^2
H-TNT	2.27	0.0003	2.67	0.990	0.96
H-TNS	2.37	0.0002	2.77	0.996	0.90

Avrami Material	$q_{e,exp}$	K_{av}	q_e (mg g^{-1})	n_{av}	R^2
H-TNT	2.27	0.209	2.27	0.20	0.97
H-TNS	2.37	0.246	2.36	0.25	0.95

are acceptable while the intraparticle diffusion model is not suitable for this system.

3.6 Reusability

The band-gaps of H-TNT and H-TNS were measured using UV-Visible spectroscopy. The obtained values are 3.4 eV and 3.5 eV, respectively. These values are too close to previously published work,[6] in which these morphologies were used as effective photocatalysts for organic dye degradation (Crystal violet). Hence, these materials can be easily recycled using UV irradiation, where the formed reactive oxygen species can easily degrade methylene blue to CO_2 and water.[38]

4. Conclusion

In the current study, titanate nanotubes (H-TNT) and titanate nanosheets (H-TNS) were developed and characterized. In order to explore their adsorption mechanism toward the cationic methylene blue dye, the maximum adsorption capacities of H-TNT and H-TNS are 7.25 and 6.67 mg g^{-1}, respectively, and the adsorption modeling has been carried out using the two traditional models; Langmuir and Freundlich. The results showed that both H-TNT and H-TNS followed the Freundlich model. The adsorption kinetics was studied using five kinetic models: *i.e.*, pseudo 1st order model, pseudo 2nd order model, intraparticle diffusion model, Avrami model, and mixed 1st and 2nd order model. However, intraparticle diffusion is not the controlling step in the adsorption process under study. During the adsorption arrays, unfamiliar behaviour of the MB spectra was detected where the standard spectrum was changed continuously. The morphology of the nanomaterials and the initial concentration of the dye play an important role in the adsorptivity process. In the case of H-TNT the monomers are the predominant species at a lower concentration (5 and 10 mg L^{-1}) while in H-TNS, the monomers are the predominant at a higher concentration (30 mg L^{-1}). Consequently, some experiments have been carried out to study the reasons for this behaviour and it can be concluded that the spectrum of the methylene blue dye is affected by the variation in dye concentration and solution temperature. So, it is highly recommended to perform a full scan to the MB dye spectra during analysis to consider the presence of the dye molecules in the monomer or dimer form in addition to defining the maximum absorbance of the dye solution at specific operating conditions.

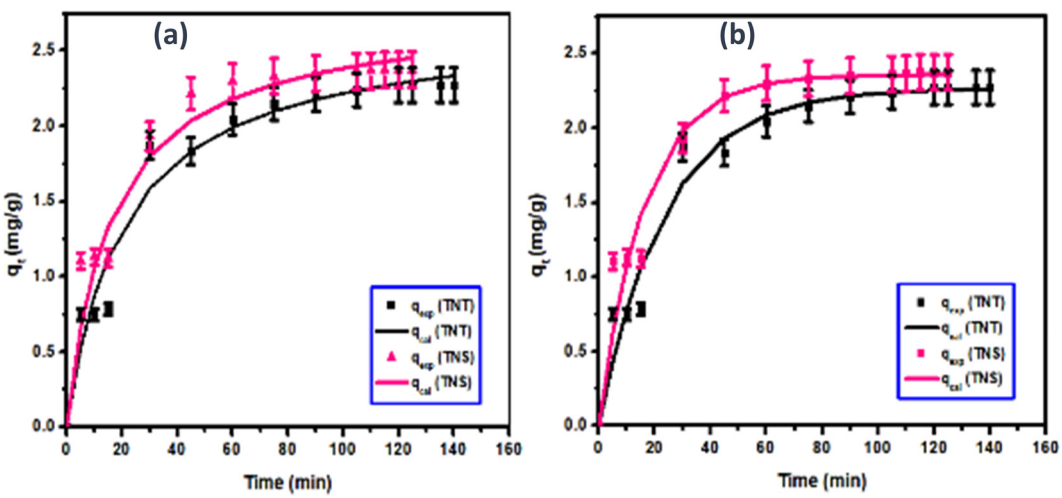

Fig. 11 Fitting of the three parameters-models: Avrami and mixed 1st and 2nd order models to the experimental studies for the adsorption of MB onto H-TNT and H-TNS.

Conflicts of interest

The authors have no relevant financial or non-financial interests to disclose.

References

1 S. Khan, M. Naushad, A. Al-Gheethi and J. Iqbal, Engineered nanoparticles for removal of pollutants from wastewater: Current status and future prospects of nanotechnology for remediation strategies, *J. Environ. Chem. Eng.*, 2021, **9**(5), 106160.

2 M. E. Elkartehi, R. Mahmoud, N. Shehata, A. Farghali, S. Gamil and A. Zaher, LDH nanocubes synthesized with zeolite templates and their high performance as adsorbents, *Nanomaterials*, 2021, **11**(12), 3315.

3 R. Saleh, A. H. Zaki, F. I. A. El-Ela, A. A. Farghali, M. Taha and R. Mahmoud, Consecutive removal of heavy metals and dyes by a fascinating method using titanate nanotubes, *J. Environ. Chem. Eng.*, 2021, **9**(1), 104726.

4 A. Tkaczyk, K. Mitrowska and A. Posyniak, Synthetic organic dyes as contaminants of the aquatic environment and their implications for ecosystems: A review, *Sci. Total Environ*, 2020, **717**, 137222.

5 A. M. Elgarahy, K. Z. Elwakeel, S. H. Mohammad and G. A. Elshoubaky, A critical review of biosorption of dyes, heavy metals and metalloids from wastewater as an efficient and green process, *Clean. Eng. Technol.*, 2021, 100209.

6 S. Rashad, A. H. Zaki and A. A. Farghali, Morphological effect of titanate nanostructures on the photocatalytic degradation of crystal violet, *Nanomater. Nanotechnol.*, 2019, **9**, 1847980418821778.

7 A. A. Abdel-Khalek, S. A. Mahmoud and A. H. Zaki, Visible light assisted photocatalytic degradation of crystal violet, bromophenol blue and eosin Y dyes using AgBr-ZnO nanocomposite, *Environ. Nanotechnol., Monit. Manage.*, 2018, **9**, 164–173.

8 A. A. Farghali, A. H. Zaki and M. H. Khedr, Control of selectivity in heterogeneous photocatalysis by tuning TiO2 morphology for water treatment applications, *Nanomater. Nanotechnol.*, 2016, **6**, 12.

9 A. H. Zaki, S. Adel, A. El-hafiez, M. Mahmoud and A. A. Abdel-Khalek, Improved production of titanate nanotubes by hydrothermal method for adsorption of organic dyes, *Beni Suef Univ. J. Basic Appl. Sci.*, 2021, **10**(1), 1–8.

10 M. R. Rahman-Setayesh, A. Rahbar Kelishami and H. Shayesteh, Equilibrium, kinetic, and thermodynamic applications for methylene blue removal using Buxus sempervirens leaf powder as a powerful low-cost adsorbent, *J. Part. Sci. Technol.*, 2019, **5**(4), 161–170.

11 H. Shayesteh, A. Ashrafi and A. Rahbar-Kelishami, Evaluation of Fe3O4@ MnO2 core-shell magnetic nanoparticles as an adsorbent for decolorization of methylene blue dye in contaminated water: synthesis and characterization, kinetic, equilibrium, and thermodynamic studies, *J. Mol. Struct.*, 2017, **1149**, 199–205.

12 R. Nodehi, H. Shayesteh and A. Rahbar-Kelishami, Fe3O4@ NiO core–shell magnetic nanoparticle for highly efficient removal of Alizarin red S anionic dye, *Int. J. Environ. Sci. Technol.*, 2022, **19**(4), 2899–2912.

13 A. Zaher and N. Shehata, Recent advances and challenges in management of urea wastewater: A mini review, *IOP Conf. Ser. Mater. Sci. Eng.*, IOP Publishing, 2021, p. 12021.

14 N. Shehata, E. T. Sayed, M. A. Abdelkareem, T. Wilberforce and A. G. Olabi, Bio-Based Adsorbents in Water/Wastewater Treatment, *Ref. Modul. Mater. Sci. Mater. Eng.*, Elsevier, 2021, DOI: 10.1016/b978-0-12-815732-9.00119-4.

15 S. Mohanty, S. Moulick and S. K. Maji, Adsorption/photodegradation of crystal violet (basic dye) from aqueous solution by hydrothermally synthesized titanate nanotube (TNT), *J. Water Process Eng.*, 2020, **37**, 101428.

16 L. Xu, C. Pan, S. Li, C. Yin, J. Zhu, Y. Pan and Q. Feng, Electrostatic Self-Assembly Synthesis of Three-Dimensional Mesoporous Lepidocrocite-Type Layered Sodium Titanate as a Superior Adsorbent for Selective Removal of Cationic Dyes via an Ion-Exchange Mechanism, *Langmuir*, 2021, **37**(19), 6080–6095.

17 C. Liu, Y. Li, X. Wang, B. Li, Y. Zhou, D. Liu, D. Liu and S. Liu, Efficient extraction of antimony (III) by titanate nanosheets: Study on adsorption behavior and mechanism, *Ecotoxicol. Environ. Saf.*, 2021, **207**, 111271.

18 T. M. F. Marques, D. A. Sales, L. S. Silva, R. D. S. Bezerra, M. S. Silva, J. A. Osajima, O. P. Ferreira, A. Ghosh, E. C. Silva Filho and B. C. Viana, Amino-functionalized titanate nanotubes for highly efficient removal of anionic dye from aqueous solution, *Appl. Surf. Sci.*, 2020, **512**, 145659.

19 A. M. Tayeb, D. S. Hussein and R. Farouq, Optimization of photocatalytic degradation of methylene blue dye using titanate nanotube, *J. Nanophotonics*, 2020, **14**, 26008.

20 J. N. D. de León, J. Rojas, D. Dominguez, Y. Esqueda-Barrón, J. M. Romo-Herrera and S. Fuentes-Moyado, The effect of shape and size of 1D and 0D titanium oxide nanorods in the photocatalytic degradation of red amaranth toxic dye, *Nano-Struct. Nano-Objects*, 2021, **26**, 100738.

21 H. Yuan, S. Ma, X. Wang, H. Long, X. Zhao, D. Yang, W. H. Lo and Y. H. Tsang, Ultra-high adsorption of cationic methylene blue on two dimensional titanate nanosheets, *RSC Adv.*, 2019, **9**, 5891–5894.

22 W. Zhang, C. Huo, B. Hou, C. Lin, X. Yan, J. Feng and W. Yan, Secondary particle size determining sedimentation and adsorption kinetics of titanate-based materials for ammonia nitrogen and methylene blue removal, *J. Mol. Liq.*, 2021, **343**, 117026.

23 H. Wang, Y. Fu, T. Han, J. Wan and X. Zheng, Adsorption and photocatalytic behavior of titanate nanotubes sensitized with zinc tetra (4-carboxyphenyl) porphyrin, *RSC Adv.*, 2015, **5**(42), 33570–33578.

24 A. H. Zaki, A. A. Motagaly, R. Khaled, M. J. Lee, A. A. Farghali and N. Shehata, Economic and facile approach for synthesis of graphene–titanate nanocomposite for water reclamation, *J. Contam. Hydrol.*, 2022, 104052.

25 M. N. Subramaniam, P. S. Goh, N. Abdullah, W. J. Lau, B. C. Ng and A. F. Ismail, Adsorption and photocatalytic

degradation of methylene blue using high surface area titanate nanotubes (TNT) synthesized via hydrothermal method, *J. Nanopart. Res.*, 2017, **19**(6), 1–13.

26 L. Xiong, Y. Yang, J. Mai, W. Sun, C. Zhang, D. Wei and J. Ni, Adsorption behavior of methylene blue onto titanate nanotubes, *Chem. Eng. J.*, 2010, **156**(2), 313–320.

27 C. K. Lee, S. S. Liu, L. C. Juang, C. C. Wang, M. D. Lyu and S. H. Hung, Application of titanate nanotubes for dyes adsorptive removal from aqueous solution, *J. Hazard. Mater.*, 2007, **148**(3), 756–760.

28 N. Florence and H. Naorem, Dimerization of methylene blue in aqueous and mixed aqueous organic solvent: A spectroscopic study, *J. Mol. Liq.*, 2014, **198**, 255–258.

29 F. W. Weaver, *Studies of methylene blue monomer-dimer reaction in super-cooled glycerol*, Texas Tech University, 2003.

30 I. Langmuir, The constitution and fundamental properties of solids and liquids. Part I. Solids, *J. Am. Chem. Soc.*, 1916, **38**, 2221–2295.

31 H. M. F. Freundlich, Over the adsorption in solution, *J. Phys. Chem*, 1906, **57**, 1100–1107.

32 K. Narasimharao, L. P. Lingamdinne, S. Al-Thabaiti, M. Mokhtar, A. Alsheshri, S. Y. Alfaifi and J. R. Koduru, Synthesis and characterization of hexagonal MgFe layered double hydroxide/grapheme oxide nanocomposite for efficient adsorptive removal of cadmium ion from aqueous solutions: Isotherm, kinetic, thermodynamic and mechanism, *J. Water Process Eng.*, 2022, **47**, 102746.

33 L. P. Lingamdinne, S. K. Godlaveeti, G. K. R. Angaru, Y. Y. Chang, R. R. Nagireddy, A. R. Somala and J. R. Koduru, Highly efficient surface sequestration of Pb2+ and Cr3+ from water using a Mn3O4 anchored reduced graphene oxide: Selective removal of Pb2+ from real water, *Chemosphere*, 2022, **299**, 134457.

34 W. Plazinski and W. Rudzinski, Kinetics of adsorption at solid/solution interfaces controlled by intraparticle diffusion: a theoretical analysis, *J. Phys. Chem. C*, 2009, **113**, 12495–12501.

35 H. Shayesteh, F. Raji and A. R. Kelishami, Influence of the alkyl chain length of surfactant on adsorption process: a case study, *Surf. Interfaces*, 2021, **22**, 100806.

36 H. Shayesteh, A. Rahbar-Kelishami and R. Norouzbeigi, Evaluation of natural and cationic surfactant modified pumice for congo red removal in batch mode: Kinetic, equilibrium, and thermodynamic studies, *J. Mol. Liq.*, 2016, **221**, 1–11.

37 J. Li, J. Cai, L. Zhong, H. Wang, H. Cheng and Q. Ma, Adsorption of reactive dyes onto chitosan/montmorillonite intercalated composite: multi-response optimization, kinetic, isotherm and thermodynamic study, *Water Sci. Technol.*, 2018, **77**, 2598–2612.

38 A. H. Zaki and M. J. Lee, Effects of K+, Mg2+, Ca2+, Zn2+, La3+, Cr3+, Ce3+, Ce4+, and Mo5+ doping on the adsorption performance and optical properties of sodium titanate nanotubes, *ACS omega*, 2019, **4**(22), 19623–19634.